Near Field Maps of Xenon Ion Velocity of the SPT-140 Hall Thruster by Laser Induced Fluorescence

IEPC-2013-053

Presented at the 33rd International Electric Propulsion Conference,
The George Washington University • Washington, D.C. • USA
October 6 – 10, 2013

Edward J. Beiting[1], Rostislav Spektor[2], Kevin D. Diamant[3]
The Aerospace Corporation, P.O. Box 92957 – M2/341, Los Angeles, CA 90009, USA

and

Ron Corey[4] and Jorge Delgado[5]
Space Systems/Loral, 3825 Fabian Way, Palo Alto, CA 94303, USA

Abstract: The xenon ion velocity distribution was mapped using laser induced fluorescence between 5 mm and 250 mm from the exit of the SPT-140 Hall thruster. Measurements were made on two grids of points in which the transverse and longitudinal velocity components were measured simultaneously in a plane containing the thruster axis. Measurements on the near field grid were centered on the discharge channel between 5 mm and 25 mm downstream from the exit plane. The xenon ions accelerated from a value of 18.5 km/s at a distance of 5 mm from the channel exit to approximately 20 km/s at a distance 20 mm from the channel exit plane. The ion velocities decreased from their peak value by 2-5% at a distance of 250 mm from the exit. The thruster showed a small asymmetry in the direction with respect to the thruster axis. No significant swirl was observed. The near field velocity values were used to calculate the electric field near the channel exit. Significant plasma pressure tensor effects were inferred from these calculations.

Nomenclature

c	=	speed of light (3.00×10^{8} m/s)
e	=	electron charge (1.6022×10^{-19} C)
E	=	electric field (V/m)
$f(v)$	=	distribution of Xe+ velocities
m	=	mass of the electron (9.1095×10^{-31} kg)
$\Delta\nu$	=	observed frequency shift from the zero velocity frequency (Hz)
v	=	velocity of Xe ion (m/s)
ν_{12}	=	zero velocity absorption frequency (Hz)
t	=	*time (s)*
x,y,z	=	Cartesian coordinates (m)

[1] Senior Scientist, Propulsion and Plasma Science Department, edward.j.beiting@aero.org
[2] Research Scientist, Propulsion and Plasma Science Department, rostislav.spektor@aero.org
[3] Research Scientist, Propulsion and Plasma Science Department, kevin.d.diamant@aero.org
[4] SPT Subsystem Lead Engineer, Propulsion Products, corey.ron@ssd.loral.com
[5] SPT Subsystem Responsible Engineer, Propulsion Products, delgado.jorge@ssd.loral.com

I. Introduction

As part of a comprehensive evaluation of the SPT-140 (QM-2) Hall thruster for SSL, the xenon ion velocity distribution was mapped using laser induced fluorescence (LIF). The test objectives of this evaluation were to measure thruster performance and plume properties at a discharge voltage of 300 V at 3.0 kW and 4.5 kW using xenon propellant. Other results from this evaluation including measurements of thrust, specific impulse, thrust efficiency, ion flux and charge state, beam energy distributions, plasma potential, electron temperature and density, are available[1] as well as a measurement of the of neutral xenon density in the thruster near-field plume.[2] Of special note, a study of the variation of key parameters with facility pressure was made.[1]

The LIF diagnostic allows unperturbed measurements of the Xe+ velocity distribution much closer to the exit of the thruster than is possible with physical probes. Physical characteristics of the thruster operation can be inferred from a closely spaced grid of velocity measurements if made within a few millimeters of the channel exit. These characteristics include maps of the acceleration, electric field, and plasma pressure effects. Furthermore, these LIF measurements can be extended to positions where probe diagnostics can operate, allowing continuous observation from the very near field to the far field. In this work Xe+ velocity distribution were measured on a fine grid from 5 mm to 25 mm in front of the channel exit and on a course grid from 50 to 250 mm from the thruster. These measurements were made for both the 3.0 kW and 4.5 kW operating modes of the SPT-140. Although LIF measurements were made previously on an early developmental model (DM-3) of the SPT-140,[3,4] these are first LIF velocity measurements of a flight version of the thruster. Comparison of results presented here with the previous results show interesting differences.

LIF has been used numerous times previously to measure Xe+ velocity in electric thruster plumes. Some of the earliest publications relevant to this work are by Manzella[5] on a 1.5 kW SPT-100 thruster using a diode laser similar to that used here; Cedolin *et al.* [6] who used a ring dye laser on a laboratory 260 W Hall thruster, and Sadeghi *et al.*[7] who used the same method as Cedolin *et al*. on a SPT-50 thruster. Later examples can be found in the literature.

II. Facility and Method

The SPT-140 thruster was operated in a 2.4-m diameter × 9.8-m long cryopumped vacuum chamber. Two reentrant cryopumps were on the end dome behind the thruster, two more reentrant pumps were in the beam dump region, and four 1.3-m cryotubs were mounted on the cylindrical wall of the chamber adjacent to the thruster. The base pressure with no gas load and all 8 pumps running was approximately 1.4×10^{-7} Torr after 16 hours of pumping. Background pressure was measured with a Stabil-Ion gauge located on the tank wall adjacent to the thruster. Facility pressures corrected for xenon during thruster operation were 8.46×10^{-6} and 1.14×10^{-5} Torr with the SPT-140 operating at 3.0 and 4.5 kW, respectively. Additional facility details can be found elsewhere.[1]

The LIF instrument used here is an update versions of that used previously.[3] In this method, the 5d $^4F_{5/2}$ – 6p $^4D_{5/2}$ / 6p $^4D_{5/2}$ – 6s $^4P_{3/2}$ transitions were excited using a commercially available tunable diode laser and the absorbed laser emission near 835 nm fluoresced in the visible at 542 nm. When the laser is scanned in frequency and the exact frequency at which the laser radiation is absorbed is a function of the ion velocity component, v, along the direction of the laser beam. This velocity component is calculated using the Doppler formula,

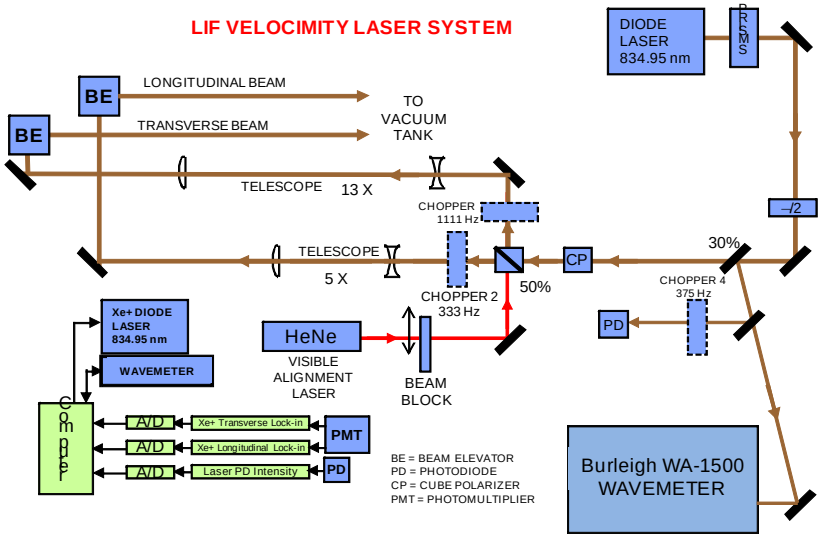

Figure 1. Instrumentation used to measure the velocity field of the SPT-140.

$$v = c\,\Delta\nu/\nu_{12} \qquad (1)$$

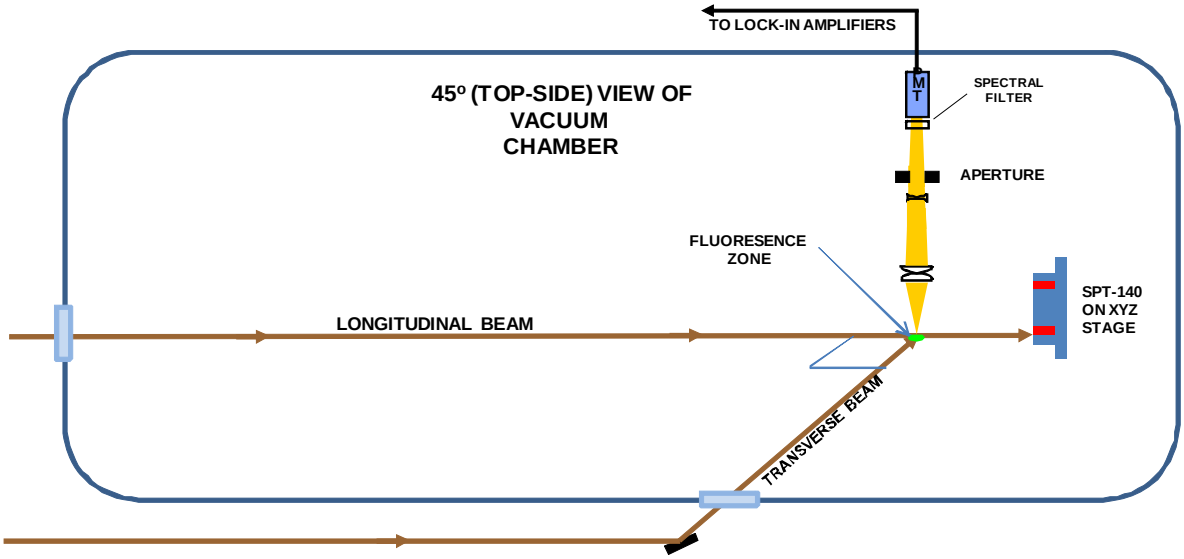

Figure 2. Plan of orthogonal beam geometry used to measure both component of the velocity simultaneously.

where ν_{12} is the zero velocity absorption frequency, $\Delta\nu$ is the observed frequency shift from the zero velocity frequency due to the absorber velocity, and c is the speed of light. For the excitation transition used here, c/ν_{12} = 835 m/s per GHz.

The instrument comprising a transmitter, wavemeter, beam transfer optics, fluorescence collection assembly, and data acquisition electronics is depicted in Figure 1. All optical components are stationary and the thruster is moved to change measurement positions. The geometry of the measurements is presented in Figure 2. The laser beams that measure the two components of the velocity are measured simultaneously. A transverse beam parallel to the exit plane of the thruster is used to measure transverse velocity. The transverse component may be either radial or azimuthal (circumferential) in the thruster coordinate system, depending on the location of the measurement point (see Figure 3). A second beam is used to measure the velocity component in the axial direction. The fluorescence, created by the two beams and registered on a single photomultiplier, is modulated by the two chopper frequencies and is separated into the two components using lock-in amplifiers.

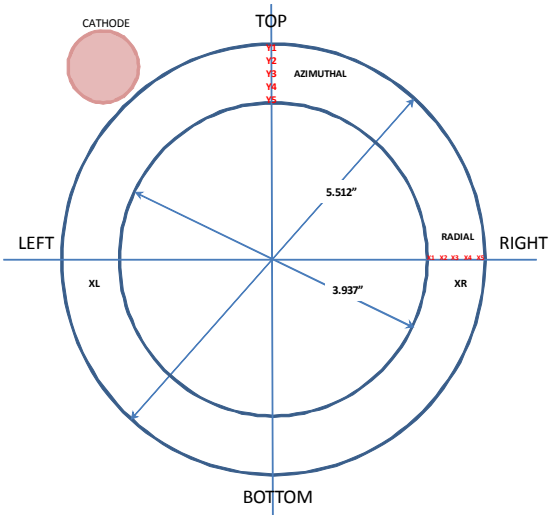

Figure 3. Front view of SPT-140 showing position of radial and azimuthal grids an position of cathode.

A three-axis motorized positioning system moved; all optical components were stationary. The Z axis (Z-stage) was along the thruster centerline, the Y axis pointed upward, and the X axis completed the right-handed set.

With the exception of the few measurements made of the azimuthal velocity shown in Figure 3, all measurements were made on two grids of points in which the transverse and longitudinal velocity components were in a plane containing the thruster axis (see Figures 4 and 5). Measurements on the near field grid were centered on the discharge channel between 5 mm and 25 mm downstream from the exit plane. Measurements on the course grid mapped the two components of the velocity along the axis of the thruster up to 250 mm from the exit plane and transversely up to 200 mm from the axis. The velocities measured near the exit plane map the ion trajectories where the magnetic field is strong and the ions are accelerating; velocities measured on the course grid provide a link to the ion energy distributions measured at 1 m from the exit plane.

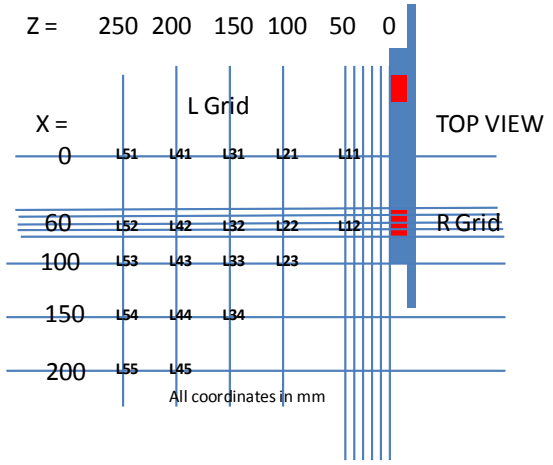

Figure 4. Scaled top view of large measurement grid.

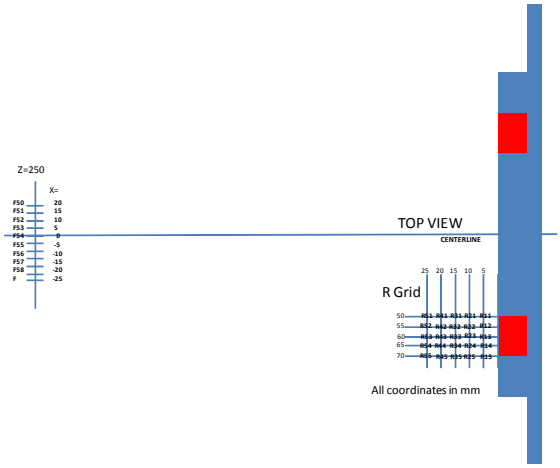

Figure 5. Scaled top view of small measurement grid.

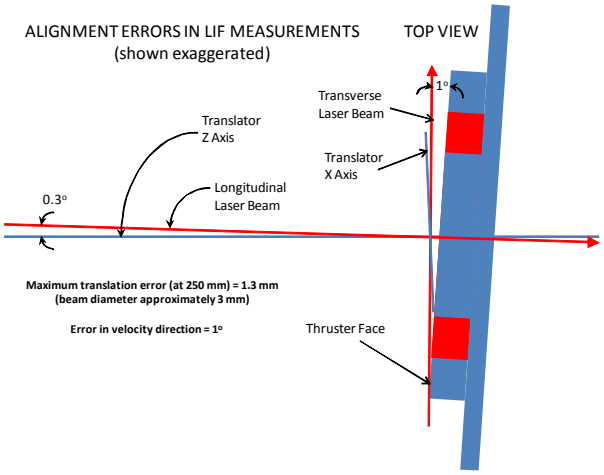

Figure 6. Alignment accuracy of SPT-140 with laser beams. Misalignments are exaggerated.

Figure 6 illustrates the accuracy of the angular alignment of the thruster with the nearly orthogonal laser beams. The face of the thruster was rotated approximately 1 degree with respect to the thruster face in the direction shown. This misalignment rotates the velocity vectors this amount with respect to the thruster axis. All data presented in this report are corrected for this misalignment. Additionally, the z-axis translation stage is misaligned with respect to the longitudinal laser beam by 0.3 degree. This results in a maximum walk off the measurement of point of less than 1.5 mm at a distance of 250 mm from the thruster, the maximum measurement distance. This error is about half the width of the laser beams and consequently not significant. The accuracy of the velocity measurements is estimated to be ±0.1 km/s. This error is largely due to the distribution of the ion velocities.

Figures 7 and 8 display combined longitudinal and transverse velocity distributions for the 3.0 and 4.5 kW data, respectively. These distributions are located in the positions of the grid shown in Figure 4 for easy reference. The coordinates corresponding to the positions on Figure 4 are shown near the top of each plot. The abscissa in these plots has been converted from frequency-offset to velocity in units of km/s using Eq. 1. In the figure, the ordinate of the plots is the strength of the fluorescence and is significant only within a single trace in an individual plot; there are longitudinal (in blue) and transverse (in green) traces in each plot and there is no relationship between the amplitude in these two traces.

The components of the velocity can be inferred from the plots in two ways. The simplest is to assign the velocity component to the peak amplitude. This works well if the trace is sharply peaked and symmetric about a single maximum. This is true near the center of the channel near the face of the thruster [positions (1,2), (2,2), (3,2), (2,3), (3,3), etc. in Figure 4]. However, moving away from this region one sees more complex distributions. These complex distributions result from ion contributions from opposite sides of the annulus as discussed previously.[3] It is better to use a weighted average of the velocity (the first moment of the distribution) i.e.

$$\mathrm{v} = \int f(\mathrm{v})\mathrm{v}d\mathrm{v} \Big/ \int f(\mathrm{v})d\mathrm{v} \qquad (2)$$

where v is the velocity component and $f(\mathrm{v})$ is the distribution. Both methods were used for each component spectrum and the results are displayed in each plot; the peak velocity is listed first and the mean is listed in the parentheses (the L subscript is used the longitudinal component). Some velocity distributions display two transverse peaks

indicating that ion populations originating from both sides of the annular channel are contributing to the fluorescence.

A more intuitive view of these velocities is shown in Figure 9. This is a vector plot of all the velocities measured on the large grid with the position of the SPT-140 shown at the bottom of the plot. For ease in viewing, the 3.0 kW and 4.5 kW data are shown on different sides of the thruster in this figure (reflected across the thruster axis) even though they were taken on the same side. The blue arrows show the 3.0 kW mean velocity vectors and the red arrows show the 4.5 kW mean velocity vectors. The green arrows show the velocity vectors inferred from the peak of the fluorescence spectra. A difference between the green arrow and its corresponding red or blue arrow is an indication of an asymmetry in the velocity distributions.

The centerline of the thruster shows an asymmetry in the center ion jet. The velocity vectors point preferentially to the left (remember the 4.5 kW red vectors have been reflected about the axis of the thruster and show the same direction of asymmetry as the 3.0 kW blue vectors). This asymmetry is not due to a misalignment of the thruster with respect to the laser beams. Had the thruster jet been symmetric, the vectors on the centerline would be vertical. This asymmetry was explored by taking a series of velocity distributions along a closely space grid, 250 mm from the face of the thruster (see Figure 5 for the positions). The spectra from this study are presented in Figure 10 and plots the components of these measurements are shown in Figure 11. In is clear from these velocity distributions that the transverse distributions are not symmetric near the centerline of the thruster except near x = -15 mm. Furthermore, although the longitudinal component of the inferred velocities is nearly constant with a value near 19.5 km/s, the transverse component is only zero at x = -25 mm and x = + 8 mm and is maximum near x = - 5 mm. These results indicate a slight misalignment of the center jet of ions with the axis of the thruster.

Figure 12 shows the inferred transverse velocity components from the velocity distributions taken along a line at the Y3 position shown in Figure 3. These data were taken to measure the azimuthal component of the ion velocity. The results indicate a small azimuthal component. This component is not significant indicating that there is effectively no swirl. The longitudinal component shows the asymptotic increase toward values between 19.5 and 20 km/s. There is no final data point for the 4.5 kW run because a power bump shut off the thruster during this acquisition sequence.

Lastly, velocity distributions were acquired on the closely spaced grid shown in Figure 5 directly in front of the channel. The velocity vectors inferred from these distributions are shown in Figure 13. Here the 3.0 kW vectors are shown in blue and the 4.5 kW vectors are shown in red. The numbers below each vector are the transverse and longitudinal mean velocity components for each position.

These data can be used to calculate a map of the electric field outside the discharge channel by noting that the force vectors are related to the acceleration through Newton's second law (**F** = m d**v**/dt). If the predominate force is the electric field then the electric field can be calculated simply from the velocity gradient, *viz.*

$$e\vec{E} = m\frac{d\vec{\mathrm{v}}}{dt} = m\left[\frac{\partial\vec{\mathrm{v}}}{\partial x}\frac{\partial \mathrm{x}}{\partial t} + \frac{\partial\vec{\mathrm{v}}}{\partial y}\frac{\partial \mathrm{y}}{\partial t}\right] = m\left[\mathrm{v}_x\frac{\partial\vec{\mathrm{v}}}{\partial x} + \mathrm{v}_y\frac{\partial\vec{\mathrm{v}}}{\partial y}\right] \tag{2}$$

where *m* and *e* are the mass and charge of the electron respectively. However if plasma pressure tensor effects cannot be neglected, then a more complex expression must be used to infer the electric field from the velocity field.[8] Here the pressure tensor is taken into account in a fully two-dimensional (2-D) electric field through the solution of the Boltzmann equation. In this calculation, the entire measured 2-D ion velocity distribution function at each physical location is used. We note that the pressure tensor can be important even when the ion flow is cold because the velocity spread results from ions being born at different potentials rather than collisional effects.

The electric field maps calculated using both the simple and more detailed method are shown in Figure 14. As can be seen, the two methods give significantly different results near the center of the channel indicating that the pressure tensor cannot be ignored in the calculations. Where these differences are large, ions migrate toward the axis of the thruster to create the center jet.

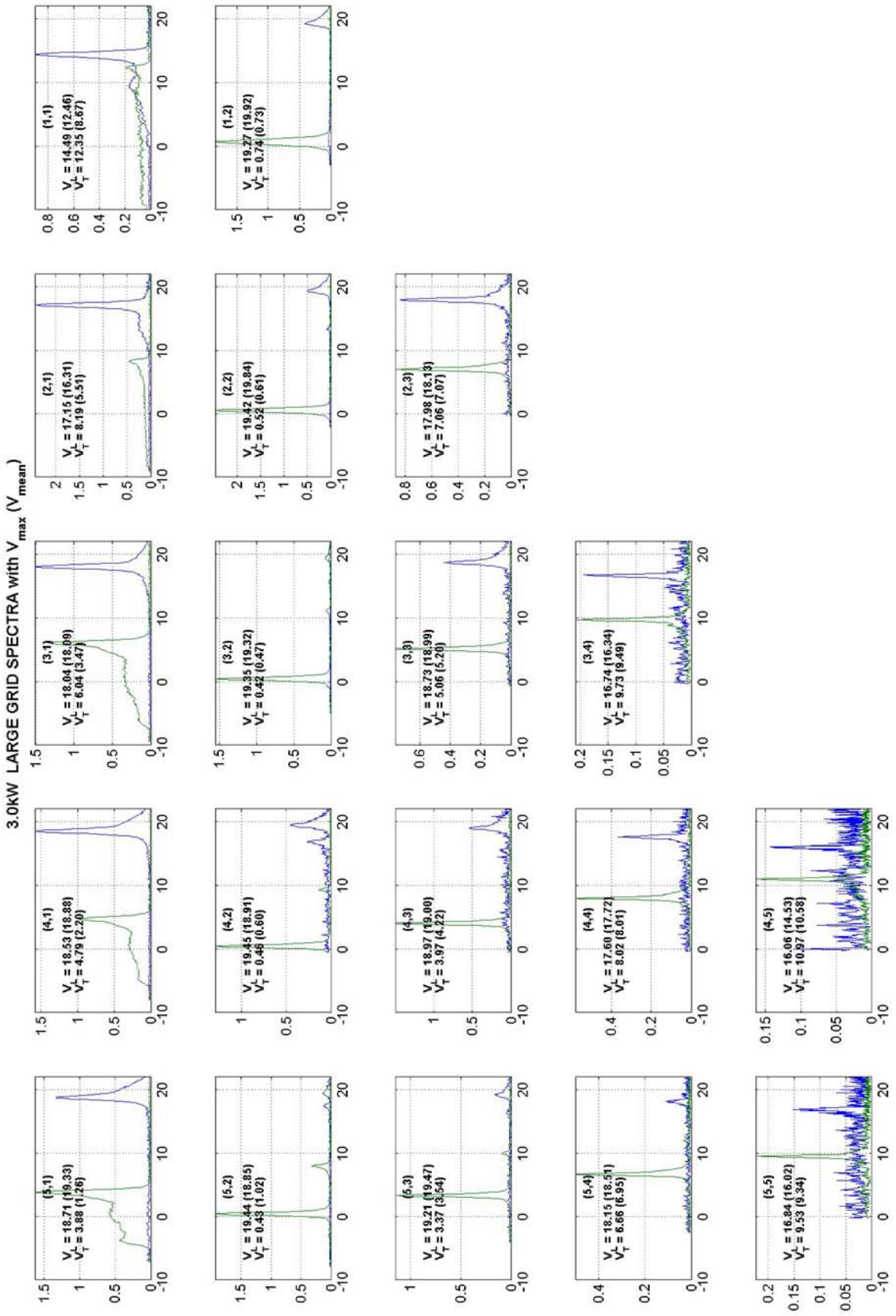

Figure 7. 3.0 kW large grid spectra with inferred velocities.

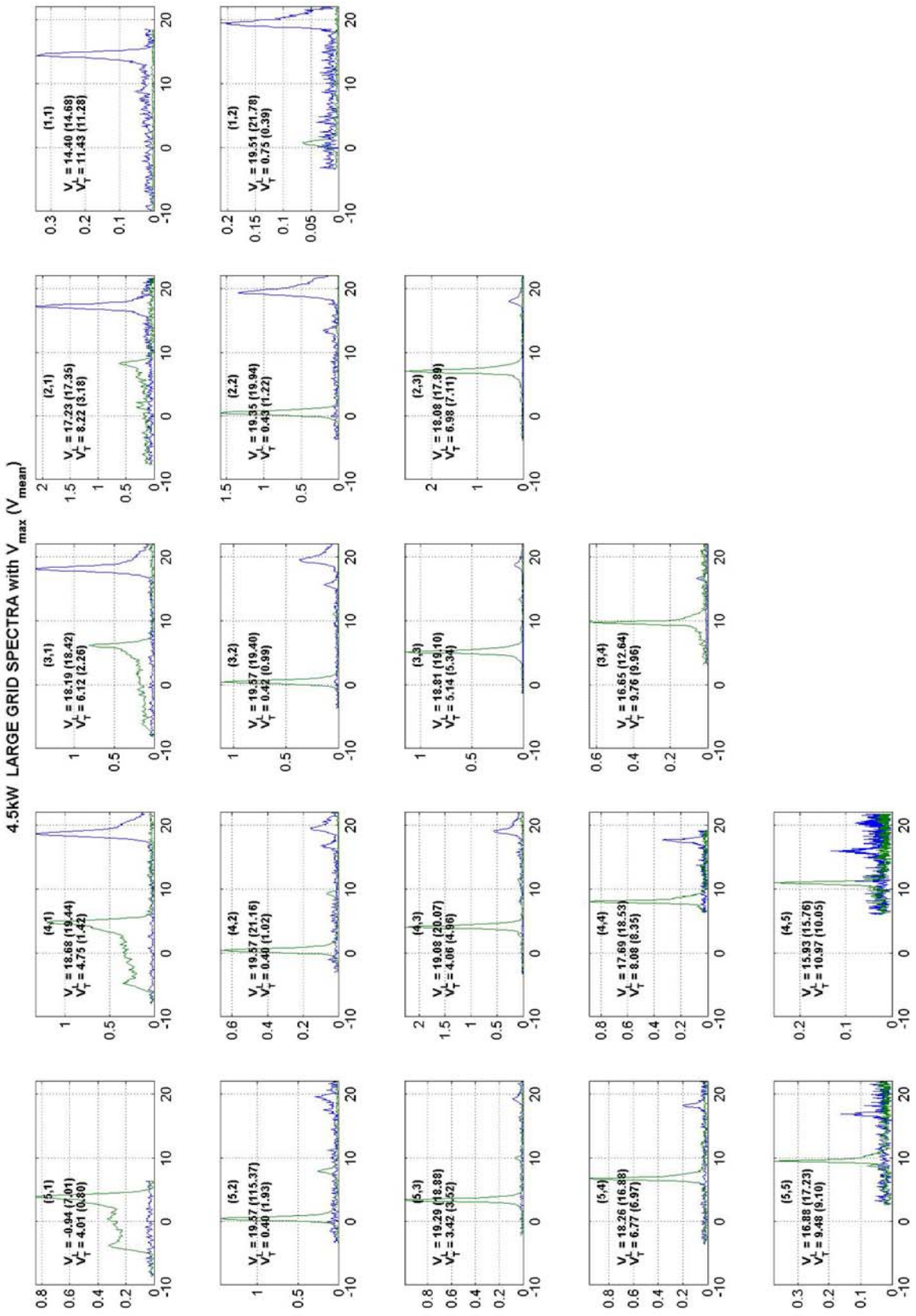

Figure 8. 4.5 kW large grid spectra with inferred velocities

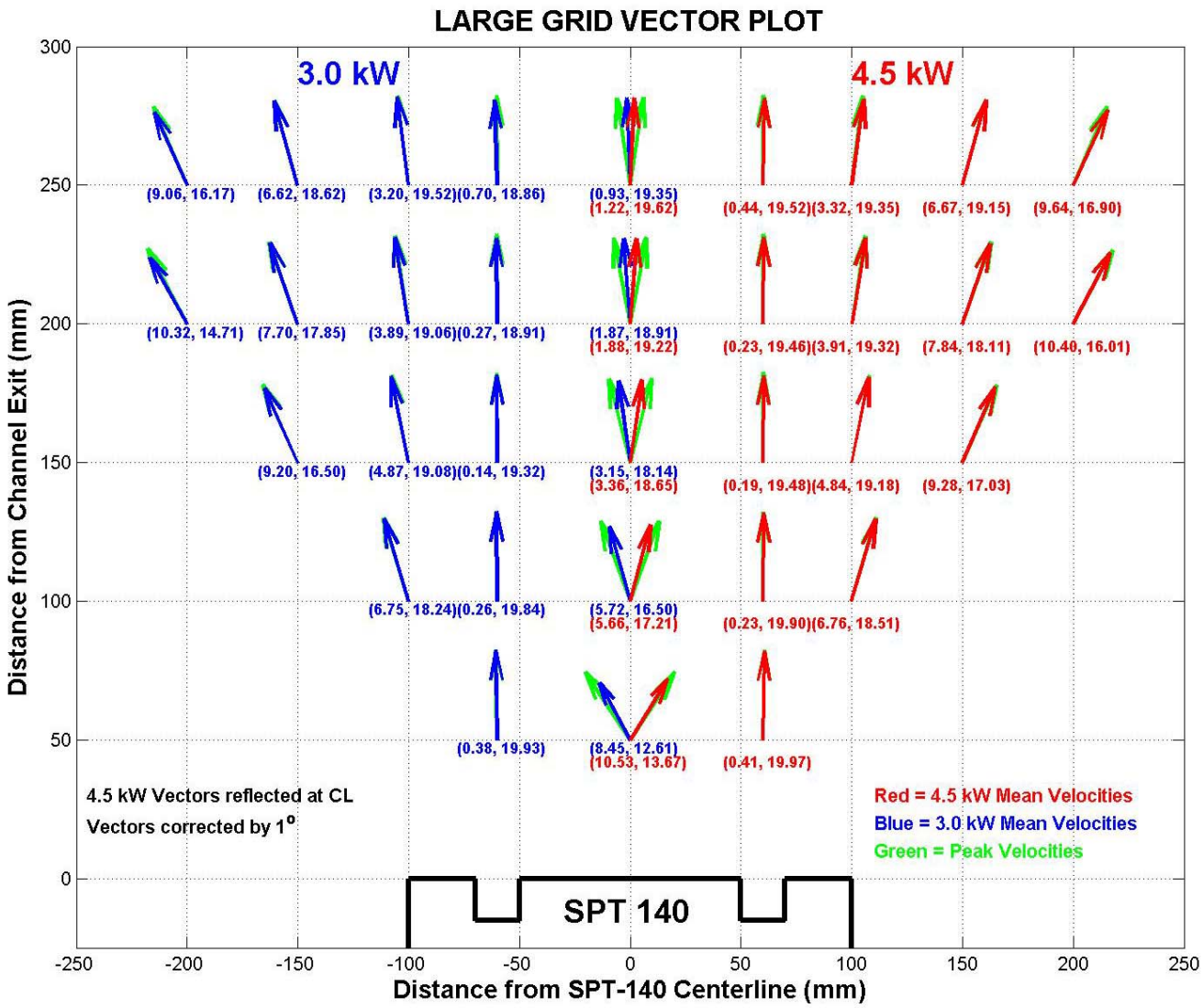

Figure 9. Velocity vector plot of all inferred velocities on the course grid.

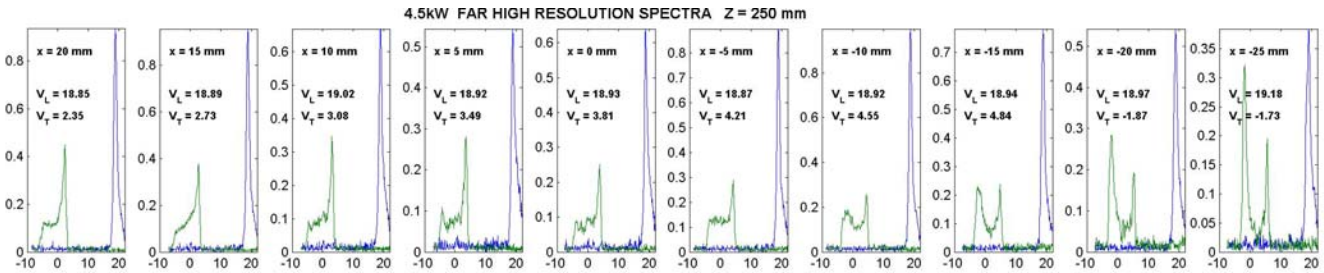

Figure 10. Closely spaced velocity distributions taken at z = 250.

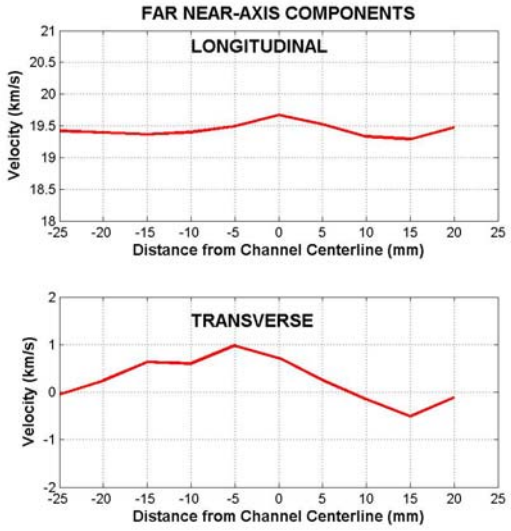

Figure 11. Mean velocities inferred from the closely spaced velocity distributions taken at z = 250

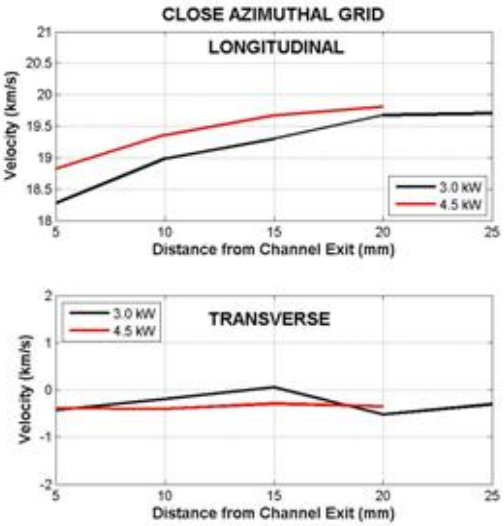

Figure 12. Azimuthal component of the ion velocity taken long the Y3 coordinate.

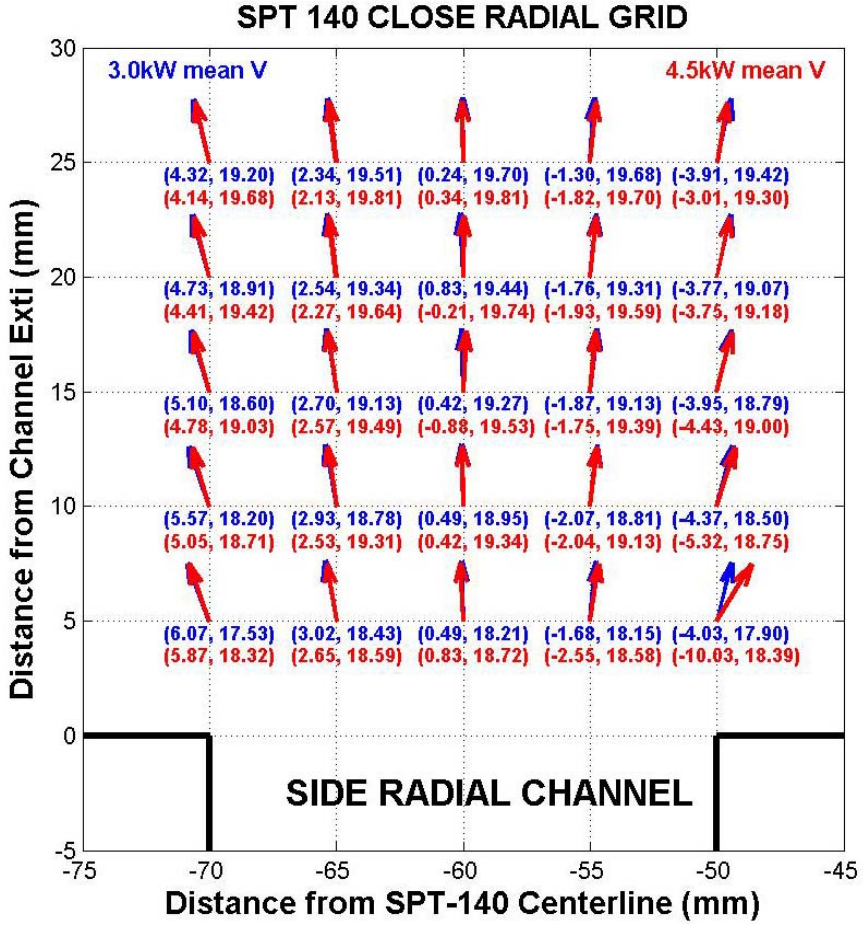

Figure 13. Velocity vectors measure near the channel exit.

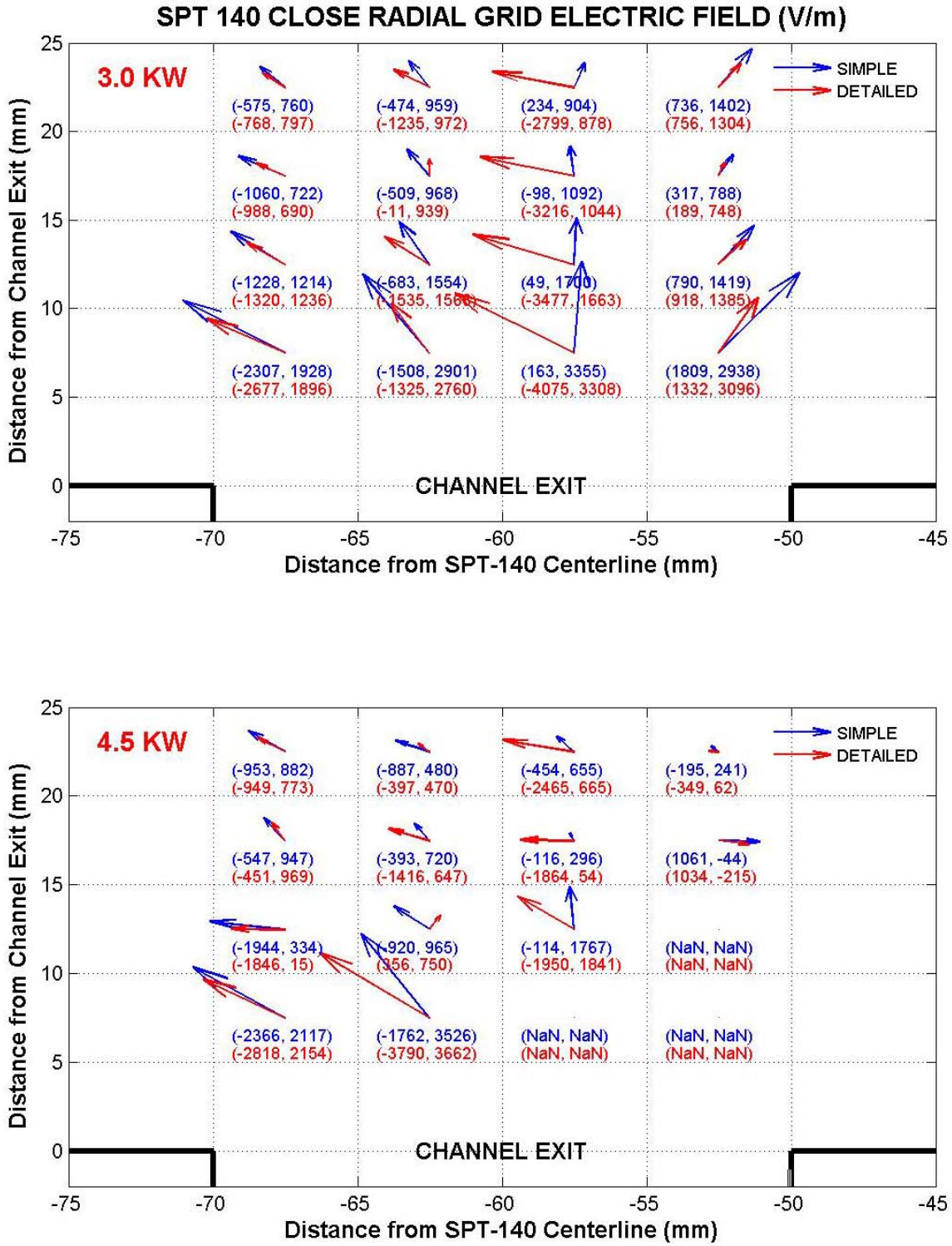

Figure 14. Electric field maps inferred from velocity fields for the 3.0 kW mode (upper plot) and the 4.5 kW mode (lower plot). The values in units of volts/meter are given below each vector.

III. Conclusions and Discussion

The velocity maps created using laser induced fluorescence showed that the xenon ions accelerated from a value of about 18.5 km/s at a distance of 5 mm from the channel exit (the closest measurement distance) to a maximum value of approximately 20 km/s a distance 20 mm from the channel exit plane. The thruster showed an asymmetry in the direction with respect to the thruster axis. No significant swirl was observed. The near field velocity values were used to calculate the electric field near the channel exit. Significant plasma pressure effects were inferred from these calculations. Assuming a peak velocity of 20 km/s, the voltage utilization efficiency is 91% for a 300 V discharge potential.

It is interesting to compare the velocity measurements of this qualification thruster QM-2 to that the of development model DM-3 for the SPT-140 made in the year 2000. We make this comparison for the magnitude of the velocities both at the centerline of the channel and the centerline of the thruster. These two comparisons are shown in Figures 15 and 16, respectively. From Figure 15 we see that acceleration in QM-2 takes place primarily before the ions exit the channel, having achieved > 90% of their final velocity just 5 mm from the channel exit. The velocity of the DM-3 is <80% of its terminal values at 5 mm. Additionally, the velocity at 50 mm is 3 – 4 % higher for the QM-2 than the DM-3. In both thrusters the acceleration takes closer to the anode when operated in its higher power mode.

A somewhat similar situation is seen with the thruster centerline velocity magnitudes shown in Figure 16. Here, however, the magnitude of the velocity in DM-3 operating at 4.5 kW is near its terminal value at 50 mm whereas appreciable acceleration is still taking place between 50 and 150 mm in this ion jet on the other three curves.

Finally, it is interesting to note from Figure 9 that the channel centerline velocities reach their maximum values near 50 mm and then these magnitudes decrease monotonically out to 250 mm, a decrease of 5% for the 3.0 kW mode and 2% for the 4.5 kW mode. This trend is not seen in the DM-3 measurements. This is likely not due to a facility pressure effect as the pressure is greater for the higher power operating mode and the facility pressure was higher for the DM-3 measurements than of the QM-2 measurements. In general, the SPT-140 shows significant improvement between the development model DM-3 and the qualification model QM-2.

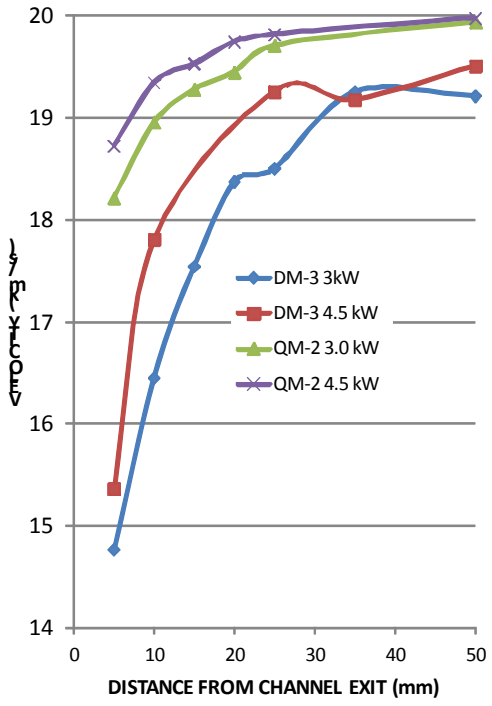

Figure 15. Channel centerline velocities.

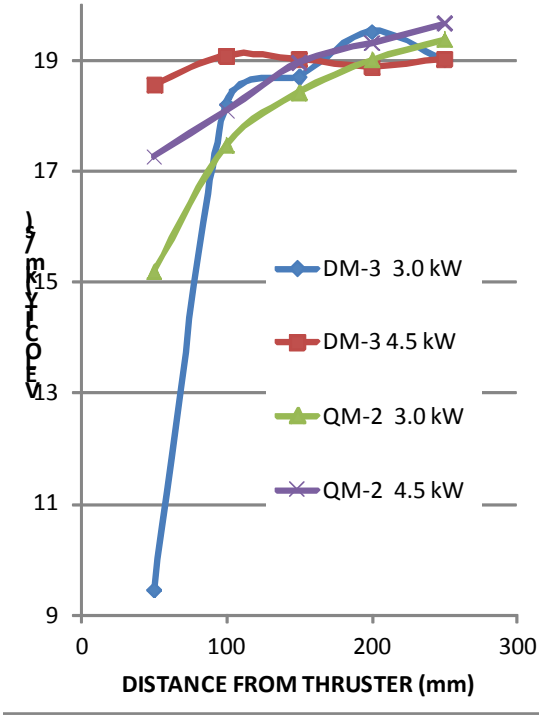

Figure 16. Thruster centerline velocities.

Acknowledgments

The authors thank Dr. Jason Young for developing much of the data logging and 3-axis translator control software used to operate the facility. This work was supported by SSL through Contract No. BPA 3221 to The Aerospace Corporation. The preparation of this manuscript was supported under The Aerospace Corporation's Sustained Experimentation and Research for Program Applications program.

References

[1] Diamant, K.D., Beiting, E.J., Crofton, M.W., Young, J.A., Spektor, R., Hsu-Schouten, A., Corey, R., and Delgado, J., "Performance and Plume Characterization of the SPT-140 Hall Thruster," 33rd International Electric Propulsion Conf., Washington, D.C., Oct. 6 – 10, 2013, IEPC-2013-xxx.

[2] Crofton, M.W., Hsu-Schouten, A.G., Young, J.A, Beiting, E.J., and Diamant, K.D., Corey, R.L., Delgo, J.J., and Jameson, K.K. "Neutral Xenon Density in the SPT-140 Near Field Plume," 33rd International Electric Propulsion Conf., 33rd International Electric Propulsion Conf., Washington, D.C., Oct. 6 – 10, 2013, IEPC-2013-xxx.

[3] Beiting, E.J. and Pollard, J.E., "Measurements of Xenon Ion velocities SPT-140 using Laser Induced Fluorescence," 3rd International Conference on Space Propulsion, Cannes, France, 10-13 Oct 2000.

[4] Pollard, J.E., and Beiting, E.J., "Ion energy, ion velocity, and thrust vector measurements for the SPT-140 Hall thruster," 3rd International Conference on Space Propulsion, Cannes, France, 10-13 Oct 2000.

[5] Manzella, D.H., "Stationary plasma thruster ion velocity distribution," 30th Joint Prop. Conf., Indianapolis, IN, June 27-29,1994, AIAA-94-3141.

[6] R. J. Cedolin, W. A. Hargus, Jr., P. V. Storm, R. K. Hanson, and M. A. Capelli, "Laser-induced fluorescence study of a xenon Hall thruster," Appl. Phys. B 65, 459-469 (1997).

[7] N. Sadeghi, N. Dorval, J. Bonnet, D. Pigache, C. Kadlec-Philippe, A. Bouchoule, "Velocity measurements of Xe+ in stationary plasma thruster using LIF," 35th Joint Propulsion Conference, Los Angeles, CA, June 20-23 1999, AIAA 99-2429.

[8] R. Spektor, "Computation of two-dimensional electric field from the ion laser induced fluorescence measurements," Phys Plasmas **17**, 093503 (2010).